EUV Generation from Lithium Laser Plasma for Lithography

Simi A. George, William Silfvast, Kazutoshi Takenoshita, Robert Bernath, Chiew-Seng Koay, Greg Shimkaveg, Martin Richardson
Laser Plasma Laboratory, College of Optics & Photonics; CREOL & FPCE
University of Central Florida, Orlando, FL, USA.

Moza Al-Rabban
Department of Physics, University of Qatar, Doha, Qatar

Howard Scott
Lawrence Livermore National Laboratory, Livermore, CA, USA.

ABSTRACT

Hydrogen-like line emission from lithium has long been considered a candidate for EUV light source for lithography. We have completed the evaluation of the potential of lithium as a laser-plasma source, both theoretically and experimentally. Theoretical calculations show optimum intensity region for lithium for attaining high conversion is close to 5.0 x 10^{11} W/cm^2, with plasma temperature near 50 eV. Experimental studies compare directly, the conversion efficiency and optimum irradiation conditions for both planar tin and lithium solid targets. Best conversion efficiency found in this study is 2% for lithium, while CE measured is better than 4% for tin target at identical experimental conditions.

Contact information: M. Richardson, College of Optics & Photonics: CREOL & FPCE, University of Central Florida, 4000, Central Florida Blvd, Orlando, FL 32816-2700, tel 407 823 6819, fax 407 823 3570, email:mcr@creol.ucf.edu

Topic: Sources
Keywords: laser plasmas, EUV Lithography, Lithium, Tin, EUV sources, EUV spectroscopy

1. INTRODUCTION

Extreme ultraviolet (EUV) lithography[1] is identified as the next generation lithography, and utilizes wavelengths in the soft x-ray region for printing integrated circuits (IC) with feature sizes below 32nm. There are a few key challenges to be solved for the successful integration of EUVL into the production line. Since EUV radiation is absorbed in nature, vacuum is required, and instead of transmissive optics, special reflective optics as well as reflective masks are needed[1, 2]. The key components of the lithographic stepper tool include, the light source, condenser with MLM collectors, patterned reflective mask on the scanning stage, reflective reduction optics, and EUV sensitive photo-resist coated wafer on the scanning stage[1]. Maximum reflectivity of EUV was found for Mo/Si multilayer mirrors (MLM) at 13.5nm[2]. A light source that meets the manufacturer requirements for source specifications at illuminator entrance[3] is one of the major challenges facing the cost-effective implementation of the EUVL stepper tool. A suitable EUV light source must be efficient, spectrally clean, with minimal or no debris emanation for preservation of the lifetime of the expensive MLM optics[3]. EUV can be generated in a number of ways, but the most

Emerging Lithographic Technologies X, edited by Michael J. Lercel,
Proc. of SPIE Vol. 6151, 615143, (2006) · 0277-786X/06/$15 · doi: 10.1117/12.660584

economical methods under consideration for lithography is the pulsed source architectures; laser produced plasmas (LPP) and gas discharge produced plasmas (DPP) [4] .

Laser plasmas are compact, intense light sources, and are advantageous due to power scalability, high repetition rates thus greater dose stability, small source size with large solid angle for collection, and energy stability. Few materials are efficient emitters of 13.5 nm radiation and currently three sources are being favoured for EUV, they are Xenon[5, 6], Tin[6], and Lithium[7]. Of these, tin and lithium targets, are expected to produce output power levels needed. Cymer, the leading industrial light source supplier, has chosen lithium LPP as the primary EUV source to use with their excimer laser systems for high volume manufacturing (HVM) [8]. Here, we present a direct comparison of EUV emission from tin and lithium planar solid targets, for a variety of experimental parameters. Through detailed spectroscopic studies, optimum EUV emission conditions can be isolated for both targets, and compare the efficiency of both targets. For laser plasmas the efficiency of the light source or the conversion efficiency (CE) is defined as the ratio of laser input to usable EUV energy at 13.5nm, in 2% reflectance bandwidth of the Mo/Si MLM optic.

2. EUV EMISSION FROM LASER PLASMAS

Focused laser radiation on target surface creates hot-dense plasma with temperatures sufficient enough to produce emission in the soft x-ray region of the electromagnetic spectrum. Laser plasma emission characteristics are directly dependent on the plasma temperature and density resulting from the laser beam interaction with the target surface. Laser wavelength, target material, and geometry are parameters that affect the plasma density, due to the variations in optical coupling efficiency. Plasma temperature and density vary in time and distance, as well. Optimizing emission from plasmas to a specific wavelength means isolating temperature and density condition ideal for that emission, which can be achieved using spectroscopy.

For temperature and density calculations from the spectroscopic quantities, few assumptions are made about the laser plasmas. We assume optically thin plasma, isotropy of emission, and the existence of local thermodynamic equilibrium (LTE). At high enough densities ($>10^{18}$cm^{-3}) conditions for LTE are valid, plasma temperatures can be calculated quite accurately for line emission from lithium, assuming that we know the plasma density. In a plasma with H-like emission, where all the transitions are to the ground state (Lyman series), the Inglis-Teller limit for last distinguishable transition can be applied to estimate the electron density. A transition from a higher state, n_i, to ground state will be resolvable if the electron density, n_e is[7, 10],

$$n_e \le \frac{Z^{9/2}}{120 a_0^3}\left(\frac{1}{n_i^2}-\frac{1}{(n_i^2+1)^2}\right)^{3/2}\left(n_i^2-1\right)^{-3/2}$$

where Z is the atomic number of the plasma source, and a_0 is the Bohr radius in appropriate units. Once the density is known, an estimate of the temperature can be obtained using ratio of intensities of emission lines originating from consecutive ionization stages[7, 9] as follows.

$$\frac{I'}{I}=\frac{f'g'\lambda^3}{fg\lambda'^3}\left(4\pi^{3/2}a_0^3 n_e\right)^{-1}\left(\frac{kT}{E_H}\right)^{3/2} Exp\left[-\frac{E'+E_\infty-E-\Delta E_\infty}{kT}\right]$$

Primes notate transition line parameters from the higher ionization stage; ΔE_∞ is the reduction of the ionization energy, E_∞, of the lower ionization stage. For a broad-band emission spectrum with unresolved transition arrays[11, 12] as in the case of tin, brute force calculations are not practical for temperature calculations and sophisticated numerical schemes are used.

3. MODELING AND SIMULATIONS

The experimental conditions were input into a 1-D Lagrangian based, hydrodynamic code to study the expansion characteristics of the plasma temperature and density for lithium. This code assumes local thermodynamic equilibrium (LTE) and isotropic emission. Oscillator strengths of transitions of lithium ionization stages were also obtained using atomic physics calculations. The transitions resulting from the excited states of the Li III ion is shown (Fig. 1). Under LTE, using the Saha equation, lithium isosequences with the fractional population for two different ion densities were calculated (Fig. 2). At larger distances

and greater time scales, the number densities of the plasma are low and the movement of the boundary region is rapid, so LTE is probably not a good assumption for accurate predictions.

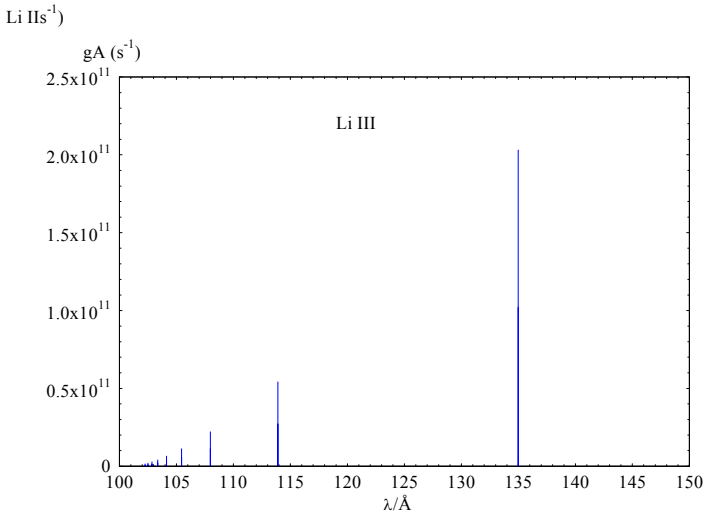

Figure 1: Atomic code calculated transitions from Li III ion

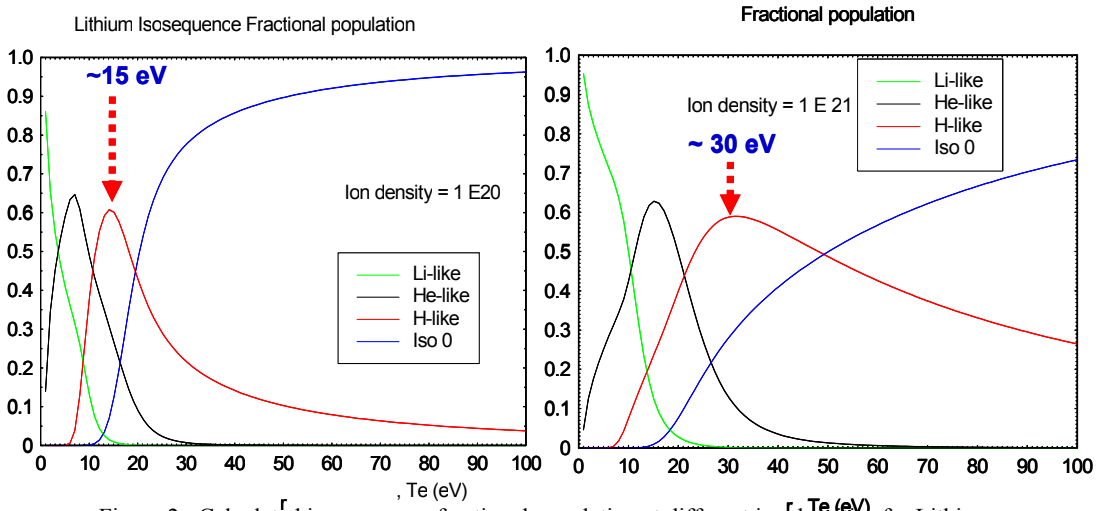

Figure 2: Calculated iso-sequence fractional population at different ion densities for Lithium

Details of the plasma processes can be better understood through the use of codes that are multi-dimensional, and treat the plasma evolution in the non-LTE, time dependant regime. CRETIN code[12, 13] is a multi-dimensional, LTE/non-LTE atomic kinetics radiation transfer code, developed at Lawrence Livermore National Laboratory (LLNL) for modeling laser plasmas. Energy transfer processes from laser to target such as inverse bremsstruhlung and resonance absorption, temporal evolution of plasma determined by the hydrodynamic and electron temperature calculations, and detailed calculations on atomic populations are all coupled to be included in Cretin simulations. Description of plasma matter at the atomic level and transition strengths are supplied to the code as external files. Hydrodynamic inputs can be post processed from the existing 1-D code or can be calculated using lagrangian routine in CRETIN. For lithium calculations, MEDUSA output for plasma expansion was provided for cretin calculations. Detailed atomic kinetics, radiation transport, plasma temperature evolution, and time evolved spectral distribution of atomic populations are obtained. CRETIN self-consistently follows the time evolution of atomic

populations and photon distributions as radiation interacts with low-density plasma[13]. Distribution of electrons in various atomic levels, relating to each atomic state is modeled for each element in the plasma. Synthetic spectra were calculated for lithium laser plasma for a number of laser irradiance conditions, as the populations evolve in time.

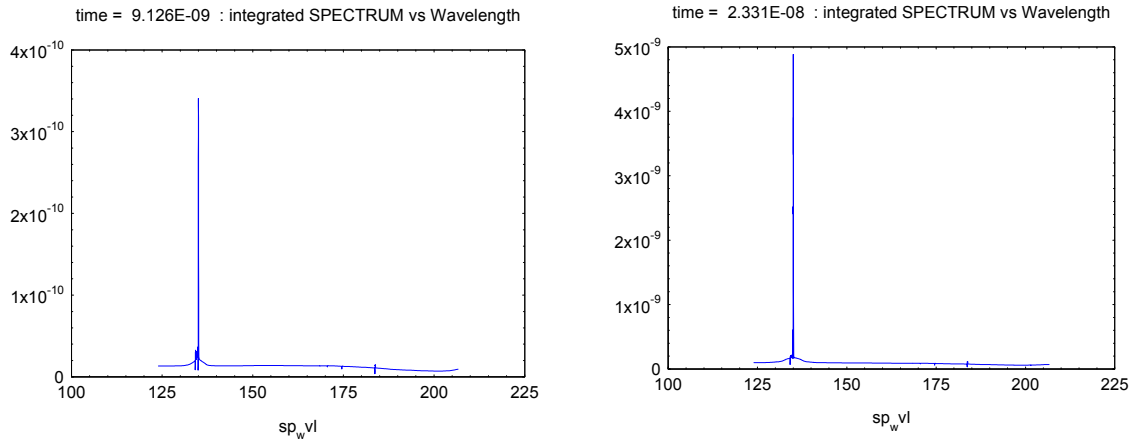

Figure 3: Calculated evolution spectral emission from lithium at laser intensity 5.0 x 10^{11} W/cm^2.

Shown (Fig. 3) is the calculated spectral emission at 13.5 nm from lithium at input laser intensity of 5.0 x 10^{11} W/cm^2 for a plasma diameter of 50 μm. Self absorption in lithium is found to be at the minimum at this intensity, with optimum plasma temperature in the region of 45-50 eV.

4. EXPERIMENTAL SET-UP

The laser used in the studies is a commercially available, Q-switched, Nd:YAG system, that can be operated at 10 Hz, 5 Hz, or 2 Hz with maximum attainable energy of approximately 200 mJ per pulse. The laser wavelength used was 1064 nm, with pulse duration (FWHM) of 10.5 ns and beam diameter at 9 mm. The beam was focused, using an anti-reflection coated Plano-convex lens with focal length of 100 mm and 50 mm diameter, on to the sample surface at an angle of 45°. Detailed map of the focal region was obtained

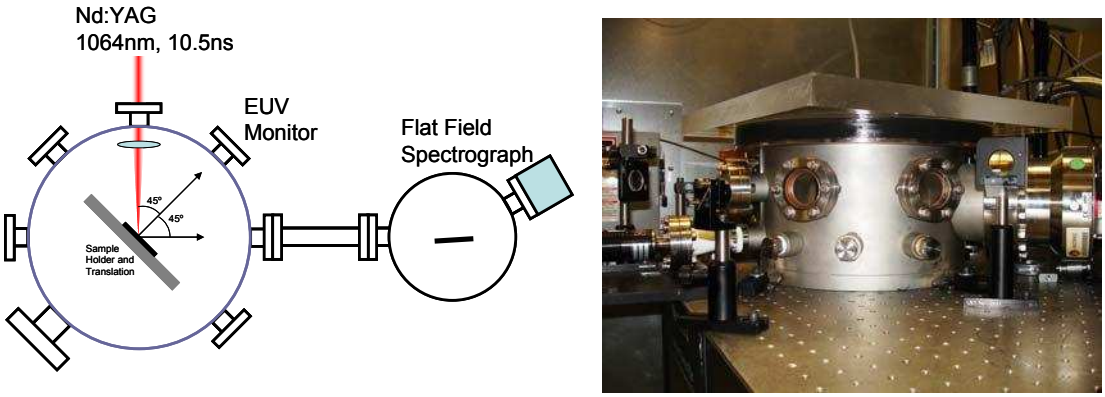

Figure 4: Experimental set-up and Chamber used

in order to calculate beam intensity for a given spectral measurement. Minimum spot size achievable is 30 μm within error limits, and the lens was translated to vary the spot size, thus giving us beam intensity variations. The chamber used for the studies is 33 cm in diameter, 18 cm in height, with eight ports separated by 45°, and eight ½ inch NPT feedthroughs. Vacuum better than 4 x 10^{-6} Torr was achieved during experiments. The experimental set-up and chamber are shown (Fig. 4).

High resolution spectra were collected using a flat-field grazing incidence grating spectrograph (FFS) [14, 15], which has a fixed entrance slit and a variably spaced 1200 lines/mm curved grating, providing a wavelength imaging range of 5 nm to 20 nm. Digital spectral images are obtained using microchannel

plates in a chevron configuration, fiber optically coupled to a 1024 x 1024, 24 μm pixel CCD. During experiments the laser operated at 2 Hz, the energy per pulse set at 65.5 mJ, and a shutter was used to obtain single shot spectra. The target surface was also translated in order to obtain a fresh surface for each measurement. To measure the EUV energy, a 22 V biased AXUV-100G detector with an efficiency of 0.24 A/W was used in combination with a 45° Mo/Si MLM, 0.5 μm Zr filter. Reflectivity data for the ML optic used in this EUV detector was obtained from National Institute for Standards and Technology (NIST). The EUV detector was placed inside the chamber and aligned normal to the target surface. The limiting aperture of the detector was determined to be the diameter of the Zr filter diaphragm mount (7.1 mm) after the MLM, located 120 mm from the plasma source resulting in a solid angle of 2.75 x 10^{-3} Sr. This detector was calibrated against the Flying Circus (FC) [6, 16, 17] EUV diagnostic instrument with calibrated optics and a solid angle of 5.0 x10^{-4} Sr, in order to ensure proper accounting of EUV energy.

The EUV energy radiated by the source across 2π str solid angle and within the 2% bandwidth (centered on 13.50nm), is given by [6, 16, 17],

$$E_{BW} = \frac{2\pi A_{scope}}{\Omega R_{scope}} \left(\frac{\int_{BW} I_s(\lambda) d\lambda}{\int_{all} I_s(\lambda) T_g(\lambda) R_{mir}(\lambda) T_f(\lambda) \eta_{diode}(\lambda) d\lambda} \right)$$

where, A_{scope} is the integrated area under the EUV signal waveform displayed on an oscilloscope, R_{scope} is the oscilloscope impedance used, $T_g(\lambda)$ is the correction for gas transmission for chamber conditions, $R_{mir}(\lambda)$ is the calibrated mirror reflectivity, $T_f(\lambda)$ is the correction for transmission of filter(s) used to block visible light from reaching detector, $\eta_{diode}(\lambda)$ is the responsivity of the AXUV detector, $I_s(\lambda)$ is measured spectral distribution EUV source in arbitrary units, and Ω is the limiting solid angle from the source to detector. Solid angle is given by $(1/4\ \pi\ D^2)/(L^2)$, where D is the diameter of the limiting aperture to the detector, and L is the distance from source to the limiting aperture.

Debris measurements[18] using mirror witness plates placed normal to the target surface 20 cm away from the plasma were conducted for both Li and Sn. The witness plates used were diced Silicon wafers, which are interchangeable during an experiment. The witness plates were exposed for 1000 laser shots, at an intensity of 1x10^{11}W/cm^2. The samples were then analyzed using white light interferometry.

5. RESULTS

Over twenty spectra were collected for a given input laser energy as a function of intensity, for both targets in order to identify optimum emission temperature of the plasma. Spectra as a function of intensity for Li and Sn solid targets are shown in fig. 1. We can clearly identify the emission lines from the He-like transition Li^{2+}(1s-2p) at 19.9 nm and H-like transitions Li^{+}(1s-2p) at 13.5 nm, Li^{+}(1s-3p) at 11.39 nm, Li^{+}(1s-4p) at 10.8 nm, in the recorded spectra (Fig. 5).

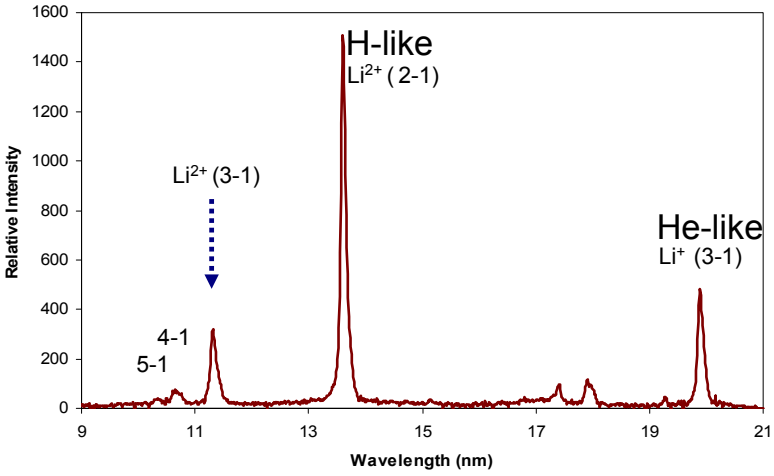

Figure 5: Observed transitions in FFS recorded lithium spectra

Maximum photon flux is found for the emission line Li^{+}(1s-2p) at 13.5 nm which will be produced at plasma temperatures greater than 10 eV and the emission to 13.5nm is maximum for the intensity region of

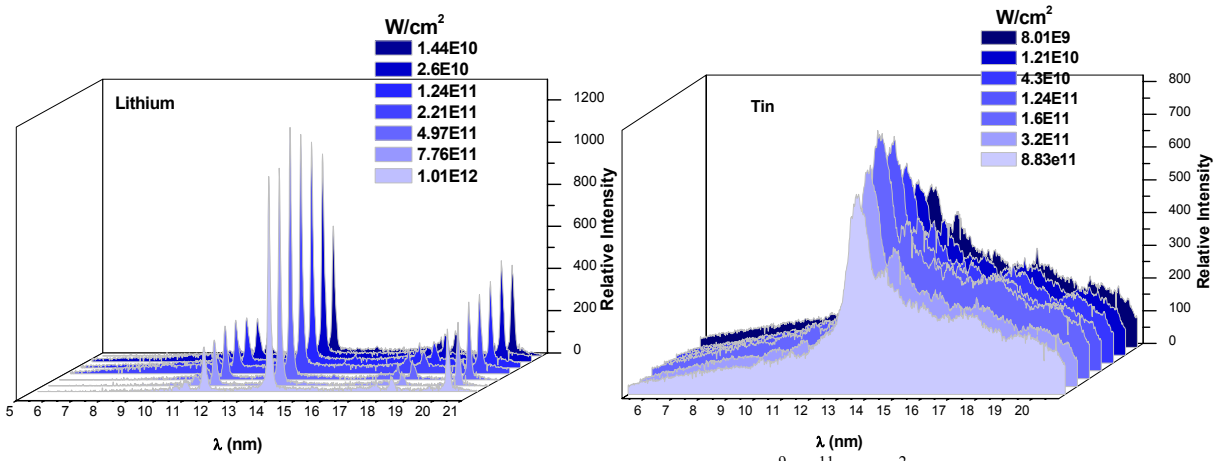

Figure 6: a) Lithium spectral distribution for laser intensities ranging from 10^{9}-10^{11} W/cm^2. Optimum region is found to be near 5 x 10^{11} W/cm^2. b) Tin spectra recorded for varying intensities with optimum emission at 1-2 x 10^{11} W/cm^2.

4.97 x 10^{11}W/cm^2. For lithium the last clearly resolvable transition, before quasi-continuum, is the Li^{+}(1s-4p) at 10.8 nm, giving an estimate of plasma electron density to be 4.6 x 10^{20} cm^{-3}. Average plasma temperature estimated for this condition is approximately 16 eV, if in LTE and close to the target surface. Tin spectra (Fig. 6) show the expected broad band emission, originating from the Sn^{12+} to Sn^{7+} ions with the ground configuration, [Kr] $4p^6$ $4d^n$, where n = 2 to 7. Most of the lines in the spectral region around 13.5 nm come from the transitions between the excited configurations, $4p^5$ $4d^{n+1}$ and $4p^6$ $4d^{n-1}$ $4f$ [1] [11, 12]. Maximum emission at 13.5 nm is found to be at intensities near 1.6 x 10^{11}W/cm^2 with plasma temperature around 30 eV, obtained using numerical simulations. Both data sets show similar behaviour, where the emission into 13.5 nm decreases with higher than optimum intensity.

Calibrated CE measurements were completed for each spectral measurement thus providing a detailed map of the EUV emission with respect to intensity for both Sn and Li (Fig. 7). Gas transmission was neglected in the CE calculations, since EUV absorption is minimal with high vacuum. Highest CE measured was 2.1% for Lithium at an intensity of 1.6 x 10^{11} W/cm^2. The tin signal collected by the photodetector was almost 5 times more than the lithium signal. We account this to the fact that we are using a mirror with a 45^{0} angle of incidence, thus passing a larger bandwidth into the detector, consequently larger conversion efficiency values. For tin target, the highest CE obtained with mirror bandwidth corrections is 4.0%, at intensity near 1.2 x 10^{11} W/cm^2.

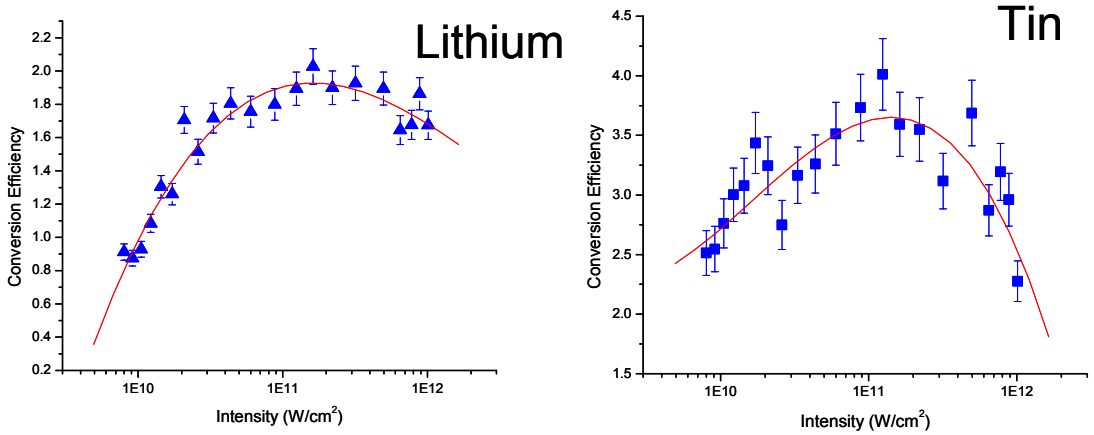

Figure 7: Conversion efficiency as function of intensity for a) Lithium b) Tin

Witness plate tests for debris were completed at 20 cm from the source, for a total of 1000 laser shots for both Li and Sn at an intensity of $1x10^{11}W/cm^2$. There are noticeable differences between the impact debris from the two targets have on the sample surface (Fig. 7). The lighter lithium ions with higher velocity shatter the mirror surface upon impact, while the tin ions mostly deposit on the surface without damaging it. The lithium deposits were smaller in size than the tin particles on the mirror surface. Analyses of the witness plate for lithium show a spray of debris on the surface. Almost all of the lithium debris are in clusters and are embedded into the Si wafer surface resulting in craters that are a few nanometers to 300 nm in depth. A few of the deepest craters have large diameters measuring approximately 50 μm. Tin samples show nearly even coating of tin across the surface of the Si wafer, with some surface damage found at the center of the wirness sample. The depth measured for tin at sample center is near 450 nm with a diameter about 30 μm. Tin samples also show tin debris adhered to the surface, that are about 40 μm in diameter, and these may respond well to surface cleaning methods.

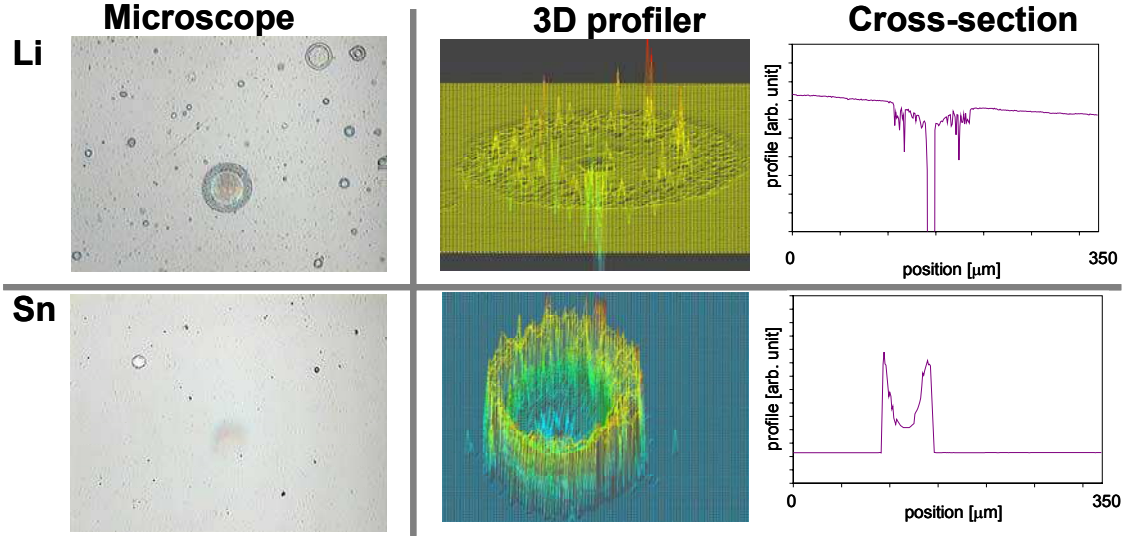

Figure 8: Debris comparison between witness plate samples obtained from tin and lithium

6. SUMMARY

Sn and Li laser produced plasmas have proven to be viable, efficient sources for EUV. Single, bright line emission from lithium at 13.5 nm makes this source a strong candidate for lithography light source. In addition, lithium is spectrally clean requiring no additional spectral purity filters, and it is abundant in nature. It is disadvantageous in that it is difficult to handle, and oxidizes easily. Tin is much easier to use, but not as abundant as lithium. UTA emission in tin is naturally brighter than single line emission, leading to higher conversion efficiencies, but it also leads to spectral purity issues.

Aside from achieving high power levels, both source schemes suffer from debris issues. Ions, particulates, and dust from coming off the plasma can damage the surface layers of the mirror, reducing the reflectivity of MLM, thus decreasing the source lifetime. EUV lithography tool design requires high repetition rate, and mass limited targets to minimize debris emanated from source. Tin-doped mass limited micro-plasma EUV source developed at UCF is considered to be well suited for use as the next generation EUV source. Our studies have shown high conversion efficiency for this source[6], with minimal tin usage. Extensive data collected for different mitigation schemes[18] show promising results for the tin droplet target, as well.

ACKNOWLEDGEMENTS

The authors would like to acknowledge the technical support from Somsak Teerawattanasook, Jose Cunado, Ji Yeon Choi, and Dr. Steve Grantham. We would like to thank Dr. Vivek Bakshi for the support of our program. Funding for this project is provided by the state of Florida.

REFERENCES

1. C. W. Gwyn, R. Stulen, D. Sweeney, and D. Attwood, JVSTB Volume 16, Issue 6, pp. 3142-3149, 1998.
2. Silfvast, W.T. IEEE J. Quantum Electron. 35, pp. 700–708, 1999.
3. Y. Watanabe, presentation at ISMT EUV source workshop, Feb. 22, 2004, proceedings available at www.sematech.org. R. Gontin. Pre.for the EUV Lith. Source work. March 2002.
4. Klosner, M. A. et. al. Optics Letters, Vol. 22, No. 1, 1999.
5. Klosner, M. A., Silfvast, W.T. Vol. 23, No. 20, 1998.
6. Koay, Chiew-Seng et. al. Proc. of SPIE, Vol. 5751, 2005.
7. D. J. O'Connell, MS thesis (UCF, Orlando, FL., 1994).
8. Fomenkov, et. al. . Symp. on EUVL (Miyasaki, Japan), 1-5 Nov. 2004. Myers et. al. Int. Symp. on EUVL (Miyasaki, Japan), 1-5 Nov. 2004.
9. Griem, H. R. McGraw-Hill, New York, 1964.
10. Griem H.R. New York, Academic Press, 1974.
11. W. Svendsen and G. O'Sullivan, *Phys. Rev. A* **50,** pp. 3710-3718, 1994.
12. M. Al-Rabban et. al. (San Jose, CA, USA, 2005), Vol. 5751, 2005.
13. H.A. Scott and R.W. Mayle, Applied Physics B, Vol. 58, pp. 35-43, 1994.
14. W. Schwanda, K. Eidmann, and M.C. Richardson, *J. X-ray Sci. and Tech*. **4**, pp. 8-17, 1993.
15. T. Kita, T. Harada, N. Takano, and H. Kuroda, *App. Opt*.**22**, pp.512-513, 1983.
16. R. Stuik, F. Scholze, J. Tummler, and F. Bijkerk, *Nuclear Inst. Method Phys. Res. A* **429**, pp. 305-316, 2002.
17. FC2: Calibration of a EUV Source at PLEX LLC (International SEMATECH Technology Transfer #04024490A-TR)
18. Takenoshita, K. et. al. J. Vac. Sci. and Tech. B Vol. 23, No. 6, pp. 2879–2884, 2005.